Quantum plasmonics and hyperbolic material for biosensing

Nathan Aubergier, Patricia Loren, Julien Guise, Franziska Braho, Pierre Fehlen, Melissa Najem, Fernando Gonzalez-Posada, Stéphane Blin, Laurent Cerutti, Rafik Smaali, et al.

Quantum plasmonics and hyperbolic material for biosensing

N. Aubergier[a], P. Loren[a], J. Guise[a], F. Barho[a], P. Fehlen[b], M. Najem[a], F. Gonzalez-Posada-Flores[a], S. Blin[a], L. Cerutti[a], R. Smaali[c], E. Centeno[c] and T. Taliercio*[a]

[a]IES, Univ Montpellier, UMR CNRS 5214, Montpellier, France; [b]NSE3 (CNRS UMR3208) Institut franco-allemand Saint-Louis; [c]Universite Clermont Auvergne, CNRS, SIGMA Clermont, Institut Pascal, F-63000 Clermont-Ferrand, France

ABSTRACT

In this work, we demonstrate that it is possible to use III-V semiconductors for plasmonics from the THz up to the mid-infrared spectral range. We have fabricated hyperbolic nano-antenna based on heavily doped semiconductors demonstrating localized plasmon modes. This hyperbolic nano-antenna is 10 times: 10 nm doped InAs / 10 nm undoped GaSb. The free carriers are confined in the 10 nm layer of InAs. The confinement shifts the effective plasma frequency of the metamaterial towards the high frequencies, extending the possibility to probe molecules until 2000 cm^{-1}, thus covering the complete fingerprint frequency range for molecular and biosensing applications. The nano-structuration of the hyperbolic material allows to access two main plasmonic resonances at 800 cm^{-1} and 2000 cm^{-1}. This bimodal property is appealing to detect and identify biomolecules over a large spectral range. With these hyperbolic nano-antennas, we can either enhance the absorption of rovibrational modes of molecules with surface-enhanced infrared absorption (SEIRA) spectroscopy[1] or enhance the thermal emission of molecules with surface-enhanced thermal emission spectroscopy (SETES)[2].

Keywords: Heavily doped semiconductor, Hyperbolic material, Biosensing, Mid-infrared spectroscopy, THz spectroscopy

1. INTRODUCTION

Plasmonics is one of the main fields of nanophotonics exploiting the coupling between photons and the collective oscillations of free carriers at metallic surfaces or nanostructures. Using heavily doped semiconductors, such as III-V materials, allows the control of the plasmonic properties of the nano-antenna adjusting the doping level of the semiconductor and the geometry of the antenna. In addition, it is possible to use other degrees of freedom to better control the plasmonic properties of the nano-antenna by the carrier quantification and hyperbolic properties. The growth techniques, such as solid source molecular beam epitaxy, allow epitaxy of the semiconductor layers at the atomic scale. This accuracy is fundamental for the design of quantum plasmonics and hyperbolic materials.

2. SAMPLE FABRICATION AND OPTICAL CHARACTERIZATION

2.1 Sample fabrication

The samples are based on antimonide alloys. They are grown by solid source molecular beam epitaxy on n-type GaSb substrate. Before growing the structure, a buffer layer of nonintentionally-doped GaSb is grown. Sample A is a 100 nm layer of Si-doped $InAs_{0.91}Sb_{0.09}$ (Fig. 1-a). This alloy is lattice-matched to the GaSb substrate allowing to decrease the density of point defects. For Sample B, 10 times GaSb 9.2 nm / InAsSb:Si 10.08 nm quantum wells are grown on the GaSb buffer (Fig. 1-b & 1-c). The GaSb/InAsSb heterostructure is a broken gap[3], that is, the conduction band energy of the InAsSb is resonant with the valence band energy of the GaSb. So, the electrons are confined in the InAsSb whereas the holes are confined in the GaSb.

The nano-antenna process flow is the following. After careful cleaning of the sample by acetone in an ultrasonic bath for 2 min, then by isopropanol (IP) alcohol for 2 min and by abundantly rinsing with IP and dried by N_2 flux, the sample is annealed for 2 min at 110°C. The photoresist AZ 2020:AZ EBR (100:80) is spread at 6000 rpm and annealed for 1 min at 110°C. E-beam lithography is performed by a modified JEOL microscope equipped with a RAITH system. It allows to pattern periodic arrays into the photoresist with widths varying from 100 nm up to 530 nm and pitches Λ of 700 nm or

930 nm. The writing parameters are 14.67 µC/cm^2, < 20pA, 20 nm, and > 1µs respectively for the dose, the beam current, the step-size, and the dwell time. The sample is, once again, annealed for 1 min. at 110°C. Then it is dipped into the developer AZ 726 for 30 s, rinsed with deionized (DI) water before being dried with N_2 flux. The remaining photoresist is the mask protecting the surface sample. The dry etching of the ribbons is performed by the induced-coupled-plasma-reactive-ion-etching (ICP-RIE) Oxford system for 2 min with the following recipes: 60°C, 5 Torr, 25 sccm, 7.5 10^{-9} Torr, 50 W, 500 W respectively for the temperature, He pressure, Ar flow, the pressure, the RF power, and the ICP power. To avoid the etching of the GaSb substrate, the dry etching is stopped a few nm above the interface between InAsSb and GaSb, and finished with a wet etching using citric acid/H_2O_2 at (2:1) for 12 s, rinsed with DI, and dried with N_2. The sample is cleaned by acetone in an ultrasonic bath for 2 min, then by isopropanol (IP) alcohol for 2 min and by abundantly rinsing with IP and dried by N_2 flux. Finally, an oxygen plasma for 3 min is performed to remove the residual photoresist.

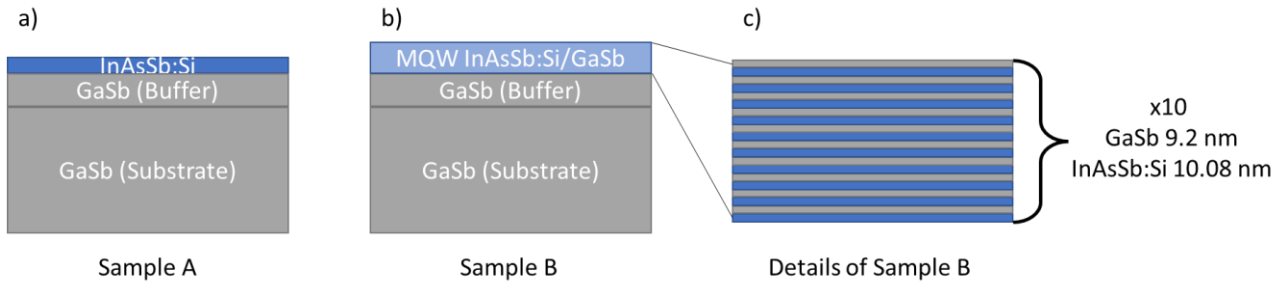

Figure 1. a) Sample A is a GaSb substrate on which a 200 nm thick buffer of GaSb is grown and 100 nm of heavily doped InAsSb:Si (n = 4.5 10^{19} cm^{-3}). b) Sample B is 10 heavily doped InAsSb:Si/GaSb quantum wells deposited on a 200 nm thick buffer of GaSb. c) Details of Sample B is 10 times 10.08 nm of heavily doped InAsSb:Si (n = 4.5 10^{19} cm^{-3}) and 9.2 nm of GaSb.

2.2 Optical characterization

The fabricated samples were characterized using a Brucker Vertex 70 Fourier transform infrared (FTIR) spectrometer. Two experimental techniques have been used. The Brewster mode experimental technique[4] allowed to extract the doping level of the InAsSb:Si. Reflectance spectra of the periodic arrays were acquired using a Hyperion 3000 microscope coupled to the FTIR.

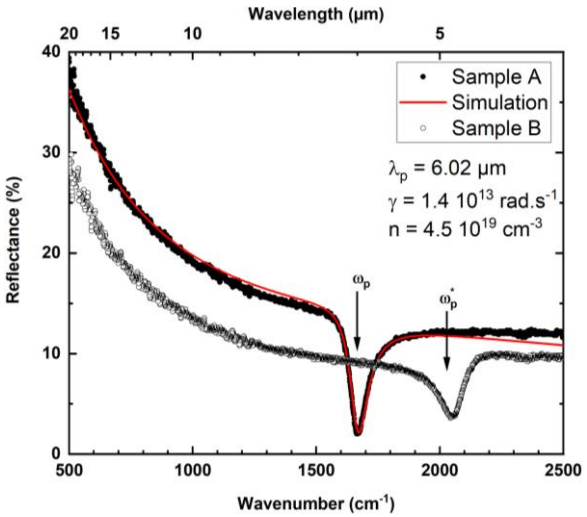

Figure 2. Brewster mode spectra of Sample A (black circles) and Sample B (black open circles). The red curve corresponds to the result of the simulation of Sample A using the Transfer Matrix Method. ω_p is the screened plasma frequency of Sample A whereas ω_p* is the effective plasma frequency of Sample B.

The Brewster mode technique allows to access the doping level by exciting a leaky mode[4] close to the screened plasma frequency, ω_p. This mode, predicted by Ferrell[5], was first observed by Steinmann[6], and McAlister and Stern[7] in an Ag

foil, and a similar mode was observed by Berreman[8] for polar materials. Its spectral signature is enhanced thanks to the cancellation of the permittivity (Epsilon near zero, ENZ, phenomena) near the frequency of the longitudinal mode of a polariton. Therefore, this mode is also termed "radiative ENZ mode" in the literature[9]. The Brewster mode technique is a reflectance experiment where the angle of incidence of the p-polarized light makes an angle of typically 60° with the normal of the sample surface.

Fig. 2 shows the reflectance spectra obtained for Sample A (black circles) and Sample B (black open circles). The narrow dips in both experimental spectra are the Brewster modes. To access the doping level, it is just necessary to measure the critical wavelength, λ_c, associated to these dips and use the abacus given in ref. 4. For Sample A, the critical wavelength is 6.00 µm and corresponds to a doping level of 4.5 10^{19} cm^{-3}, the one expected for the selected growth condition. For an accurate value of λ_c, it is possible to model the reflectance spectrum of Sample A with the transfer matrix method (TMM)[10] which is in good agreement with the experimental data (Fig. 2, red solid curve). We have used the Drude function to model the dielectric function of the heavily doped semiconductor:

$$\varepsilon(\omega) = \varepsilon_\infty \left(1 - \frac{\omega_p^2}{\omega^2 + i\gamma\omega}\right) \quad (1)$$

where ε_∞, γ, ω_p are respectively the high frequency dielectric constant, the damping constant, and the screened plasma frequency:

$$\omega_p = \sqrt{\frac{ne^2}{m^* m_0 \varepsilon_0 \varepsilon_\infty}} \quad (2)$$

which is a function of the carrier density, *n*, the electron charge, *e*, and mass in vacuum, m_0, the permittivity constant of vacuum, ε_0, and the effective mass of electron in InAsSb, *m**.

In the case of Sample B, TMM modeling of the reflectance spectrum would result in a higher doping level, higher than 1.5 10^{20} cm^{-3} which has no physical meaning because the nominal doping level is the same as Sample B's. This result can be explained by the quantum effects addressed in the next session.

3. INFLUENCE OF THE QUANTIZATION EFFECT ON PLASMONIC RESONANCES

3.1 Quantization effect

Sample B corresponds to a hyperbolic material, that is, a periodic stack of dielectric (GaSb) and metallic layers (InAsSb:Si), which sustains hyperbolic dispersion relations of electromagnetic waves propagating throughout. This kind of metamaterial features original optical properties such as ultrahigh refractive index, or negative refraction index recently observed in ZnO/(Zn,Mg)O doped quantum wells[11]. Main scientific results concerning hyperbolic materials exploit the geometrical or material parameters. However, if the thickness and the free carrier density of the metallic layer are weak enough, quantum properties, such as intersubband excitations, become crucial to consider. Intersubband excitations correspond to the electronic transition between two successive electronic states confined in a quantum well. Radiative transitions between such levels become possible only if electrons are in the first subband. In a doped quantum well, the collective excitation of a 2 dimensional electron gas, 2DEG, confined in the ground state of a quantum well[12] gives rise to an intersubband plasmon (ISBP) whose energy depends on both the plasma frequency and the energy difference between two consecutive electronic levels. When the quantum well thickness increases, a multisubband plasmon (MSBP) appears because several subbands are occupied leading to several intersubband plasmons that couple together through dipole-dipole Coulomb interactions[13]. It can be also the case of heavily doped quantum well because several subbands are occupied which is the case of Sample B. The vanishing contribution of electron confinement when the quantum well thickness increases leads progressively to the classical bulk plasmon in a semiconductor slab that is well described by the Drude model[14]. This is the case of Sample A. In Fig. 2, we can see that the quantization of the electronic states into the quantum wells of Sample B induces a blueshift (388 cm^{-1}, 11 THz or 48 meV) of the effective plasma frequency, ω_p*. We will exploit this blueshift to excite a localized plasmonic resonance associated to the multisubband plasmon (LMSBP).

3.2 Plasmonic resonances of nano-antenna

Fig. 3 are scanning electron microscope (SEM) images of the periodic arrays fabricated on Sample A. The ribbon width is controlled with the dose during the e-beam lithography process. We can see that the variation in the dose allows to adjust the ribbon width keeping constant the pitch at 930 nm. The dose varies, each 0.05, from x1.35 down to x1.1. The corresponding SEM images of the samples are gathered from a) to f). Increasing the dose reduces the ribbon width. The ribbon widths are respectively < 100nm, 150 nm, 190 nm, 300 nm, 380 nm, and 530 nm.

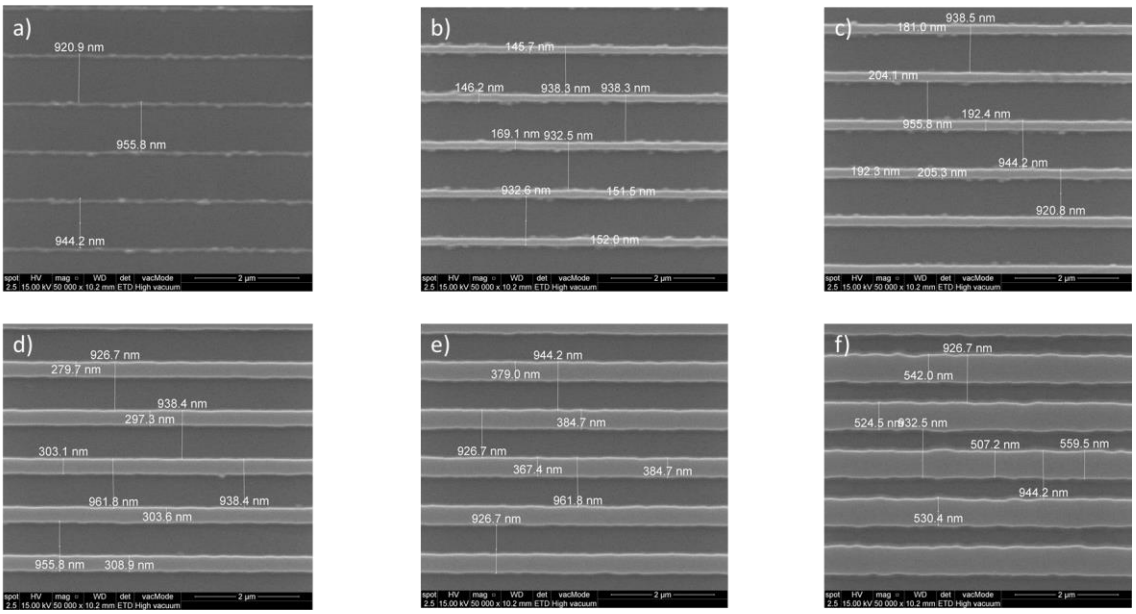

Figure 3. SEM images of 6 different samples fabricated on Sample A. The periodic arrays have the same pitch, 930 nm, and variable ribbon width. The ribbon width is controlled by adjusting the dose of the e-beam lithography, a) $w < 100$ nm, b) $w \sim 150$ nm, c) $w \sim 190$ nm, d) $w \sim 300$ nm, e) $w \sim 380$ nm, f) $w \sim 530$nm. The writing field for each pattern is 100 x 100 μm^2.

Fig. 4 shows the reflectance spectra of 6 periodic arrays with different ribbon widths varying from less than 100 nm up to 530 nm.

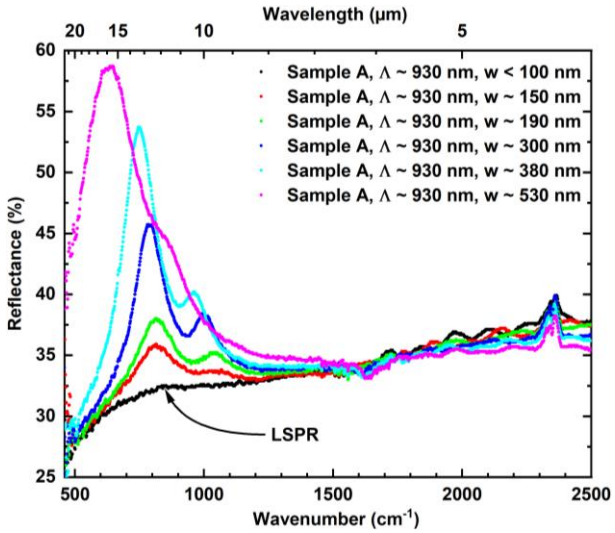

Figure 4. Reflectance spectra for the ribbon width of $w < 100$ nm (black dots), $w \sim 150$ nm (red dots), $w \sim 190$ nm (green dots), $w \sim 300$ nm (blue dots), $w \sim 380$ nm (cyan dots), $w \sim 530$nm (pink dots) fabricated on Sample A. The periodic arrays have the same pitch, $\Lambda \sim 930$ nm, and variable width.

Weak oscillations at a wavenumber larger than 1600 cm^{-1} are due to interference patterns with the sample holder. The peaks at 2350 cm^{-1} are CO_2 rovibrational modes. The main peaks spanning between 600 and 850 cm^{-1} are localized surface plasmon resonances (LSPR)[15]. The LSPR redshifts when the ribbon width increases. This is a well-known effect well described in the literature[16]. The wavelength of the LSPR mode increases with the width of the nano-antenna reducing at the same time its energy. The nano-antenna with ribbon widths of 300 and 380 nm have wavenumbers respectively of 749 cm^{-1} and 791 cm^{-1}. The increase of the peak amplitude is correlated to the increase of the ribbon width. The interaction between light and matter increases when the size of the nano-antenna is increased. The surface covered with the nano-antenna for a given pitch increases with its size.

3.3 Quantization effect on plasmonic resonances of nano-antenna

Fig. 5 are SEM images of the periodic arrays fabricated on Sample B. The pitch is $\Lambda \sim 720$ nm for all the periodic arrays. The ribbon widths span from 330 nm up to 370 nm. Even though the difference is small, it is possible to see an energy shift (proportional to the wavenumber shift) of the LSPR.

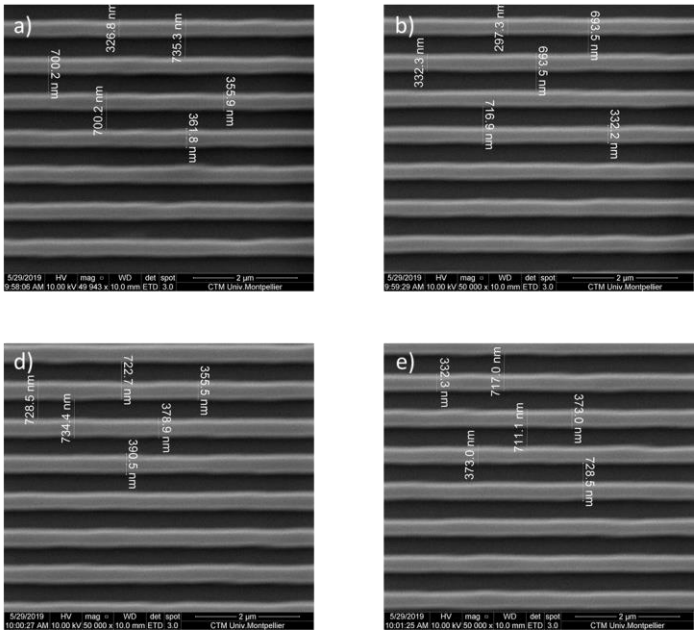

Figure 5. SEM images of 4 different samples fabricated on Sample B. The periodic arrays have the same pitch, $\Lambda \sim 720$ nm, and a quite constant ribbon width ranging from 330 nm to 370 nm.

This is what we can see in Fig. 6 which represents the reflectance spectra of the samples imaged in Fig. 5. LSPR have a wavenumber around 800 cm^{-1} as for similar periodic arrays on Sample A. For a ribbon width of 370 nm the LSPR wavenumber is 804 cm^{-1} whereas for w = 350 nm and 330 nm the wavenumbers are respectively 814 cm^{-1} and 830 cm^{-1}. This is coherent with what is expected, the larger the ribbon width, the smaller the wavenumber. However, the wavenumbers reached with this hyperbolic nano-antenna are a little bit larger than those reached with the classical plasmonic nano-antenna of Sample A (~ 750-790 cm^{-1}). This is opposite to what we can expect with hyperbolic behavior[11] which follows the in-plane permittivity:

$$\varepsilon_{in-plane}(\omega) = \frac{e_{QW}\varepsilon_{QW}(\omega) + e_B\varepsilon_B}{e_{QW} + e_B} \tag{3}$$

where e_{QW}, e_B, $\varepsilon_{QW}(\omega)$ and ε_B are respectively the thickness of the quantum well, and the barrier, and the permittivity of the quantum well and of the barrier. ε_B is assumed to be constant and ε_{QW} is equal to (1). So (3) leads us to a decrease of the wavenumber of the $\varepsilon_{in\text{-}plane}(\omega) = 0$ compared to the wavenumber of the $\varepsilon_{QW}(\omega) = 0$. To explain this blue shift, it is probably needed to consider the quantum behavior of the hyperbolic media[17]. In any case, it is necessary to consider the quantum effect to consider the new plasmonic resonance that appears at high wavenumber[17]. In Fig. 6, we can see the resonance at 1940 cm^{-1} for all reflectance spectra. We attribute this resonance to the localized plasmonic modes associated to the multisubband plasmon LMSBP. The LSMBP seems to be insensitive or less sensitive to the geometry

of the quantum hyperbolic nano-antenna. However, it opens the possibility to access the high-energy part of the fingerprint of molecules.

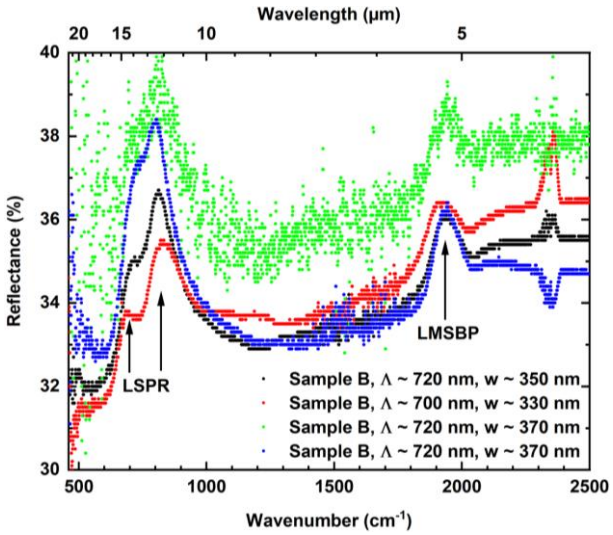

Figure 6. Reflectance spectra of periodic arrays fabricated on sample B and the SEM images are in Fig. 5. The geometries of the samples are labeled. LSPR corresponds to the "classical" plasmonic nano-antenna resonance whereas LMSBP corresponds to the plasmonic resonance due to the carrier confinement within the quantum wells.

Adjusting the quantum well width and the carrier density allows us to cover easily the spectral range from the THz to the mid-IR. Further investigations will be needed to quantify the sensing properties of this LMSBP resonance.

4. CONCLUSION

We have demonstrated that it is possible to employ III-V semiconductors for quantum plasmonics and hyperbolic metamaterials to address the mid-infrared spectral range. The hyperbolic nano-antenna fabricated with doped semiconductors using quantum effects demonstrate a bimodal behavior of localized plasmon modes (LSPR and LMSBP) that allows to access the high-energy spectral range of the fingerprint of molecules. Adjusting the carrier density with the doping level and quantum well width, it will be possible to address the spectral range from the THz up to the mid-IR. It will be needed to characterize the sensing properties of both plasmonic modes to use them to either enhance the absorption of rovibrational modes of molecules with surface-enhanced infrared absorption spectroscopy or enhance the thermal emission of molecules with surface-enhanced thermal emission spectroscopy.

ACKNOWLEDGMENTS

This work was partially funded by the French Investment for the Future Program (EquipEx EXTRA, ANR 11-EQPX-0016), the French ANR (NanoElastir ANR-19-ASTR-0003-02), the Occitanie Region (ESR_PREMAT – 00238 / Prématuration 2019 SEA). F. Pichot, J.-M. Peiris, and F. Mirabel are acknowledged for technical support at the cleanroom facilities of Université de Montpellier.

REFERENCES

[1] Barho, F. B., Gonzalez-Posada Florès, F., Cerutti, L. and Taliercio, T., "Highly doped semiconductor metamaterials for mid-infrared multispectral perfect absorption and thermal emission," Adv. Optical Mater. 1901502 (2020).

[2] Barho, F. B., Gonzalez-Posada Florès, F., Mezy, A., Cerutti, L. and Taliercio, T., "Surface-Enhanced Thermal Emission Spectroscopy with Perfect Absorber Metasurfaces," ACS Photonics 6, 1506−1514 (2019).

[3] Chang L. L., and Esaki L., "Tunnel triode-a tunneling base transistor," Appl. Phys. Lett. 31, 687 (1977).

[4] Taliercio, T., N'Tsame Guilengui, V., Cerutti, L., Tournié, E., Greffet, J. J., "Brewster "mode" in highly doped semiconductor layers an all-optical technique to monitor doping concentration," Opt. Express 22, 24294 (2014).
[5] Ferrell, R. A., "Predicted radiation of plasma oscillations in metal films," Phys. Rev. 111, 1214–22 (1958).
[6] Steinmann, W., "Experimental verification of radiation of plasma oscillations in thin silver films," Phys Rev Lett. 5, 470–2 (1960).
[7] McAlister, A. J., Stern, E. A., "Plasma resonance absorption in thin metal films," Phys. Rev. 132, 1599 (1963).
[8] Berreman D. W., "Infrared absorption at longitudinal optic frequency in cubic crystal films," Phys. Rev. 130, 2193–8, (1963).
[9] Campione, S., Kim, I., De Ceglia, D., Keeler, G. A., Luk, T. S., "Experimental verification of epsilon-near-zero plasmon polariton modes in degenerately doped semiconductor nanolayers," Opt. Express 24, 18782 (2016).
[10] Zi, J., Wan, J., and Zhang, C., "Large frequency range of negligible transmission in one-dimensional photonic quantum well structures," Appl. Phys. Lett. 73, 2084 (1998).
[11] Hierro, A., Montes Bajo, M., Ferraro, M., Tamayo-Arriola, J., Le Biavan, N., Hugues, M., Ulloa, J. M., Giudici, M., Chauveau, J.-M., and Genevet, P, "Optical Phase Transition in Semiconductor Quantum Metamaterials," Phys. Rev. Lett. 123, 117401 (2019).
[12] Ando, T., Fowler, A. B., Stern, F., "Electronic properties of two-dimensional systems," Rev Mod Phys 54, 437 (1982).
[13] Delteil, A., Vasanelli, A., Todorov, Y., Feuillet Palma, C., Renaudat St-Jean, R., Beaudoin, G., Sagnes, I., and Sirtori, C., "Charge-Induced Coherence between Intersubband Plasmons in a Quantum Structure," Phys. Rev. Lett. 109, 246808 (2012).
[14] Askenazi, B., Vasanelli, A., Delteil, A., Todorov, Y., Andreani, L. C., Beaudoin, G., Sagnes, I., and Sirtori, C., "Ultra-strong light–matter coupling for designer Reststrahlen band," New Journal of Physics 16, 043029, (2014).
[15] N'Tsame Guilengui, V., Cerutti, L., Rodriguez, J.-B., Tournié, E, and Taliercio, T., "Localized surface plasmon resonances in highly doped semiconductors nanostructures," Appl. Phys. Lett. 101, 161113 (2012).
[16] Milla, M. J., Barho, F., González-Posada, F., Cerutti, L., Bomers, M., Rodriguez, J.-B., Tournié, E., and Taliercio, T., "Localized surface plasmon resonance frequency tuning in highly doped InAsSb/GaSb one-dimensional nanostructures," Nanotechnology 27, 425201 (2016).
[17] Angela Vasanelli, A., Huppert, S., Haky, A., Laurent, T., Todorov, Y., and Sirtori, C., "Semiconductor Quantum Plasmonics," Phys. Rev. Lett. 125, 187401 (2020).